34th Annual International Conference of the IEEE EMBS
San Diego, California USA, 28 August - 1 September, 2012

Direct Inductive Stimulation for Energy-efficient Wireless Neural Interfaces

Sohmyung Ha[1], Massoud L. Khraiche[1,2], Gabriel A. Silva[1,2] and Gert Cauwenberghs[1,3]

Abstract— **Advanced neural stimulator designs consume power and produce unwanted thermal effects that risk damage to surrounding tissue. In this work, we present a simplified architecture for wireless neural stimulators that relies on a few circuit components including an inductor, capacitor and a diode to elicit an action potential in neurons. The feasibility of the design is supported with analytical models of the inductive link, electrode, electrolyte, membrane and channels of neurons. Finally, a flexible implantable prototype of the design is fabricated and tested in vitro on neural tissue.**

I. Introduction

Most wireless neural stimulators require intricate circuits for power telemetry, data telemetry, power management, clock recovery, digital control, driving stimulation pulse, etc. as shown in Fig. 1 [1]-[3]. Even neural stimulators with few channels need those circuits to generate required stimulation pulses [4],[5]. This paper investigates and analyzes direct inductive neural stimulation, bypassing the need for the extra circuits for voltage regulation and stimulation waveform shaping. Analytical models of the inductive link to the neuron, and simulated and experimental results for implantable prototypes are presented.

II. Direct Inductive Neural Stimulation

We consider a simplified architecture for wireless neural stimulation with only an LC resonant tank as shown in Fig. 2. It couples the electrode directly to the inductor coil pair, and uses the train of sine wave pulses, which are received directly from the external primary coil inductor to stimulate a neuron. For this architecture the resonance frequency of the inductive link should be same as the frequency of the stimulation pulses in the neural interface. However, the resonance frequency of the inductive link typically is over 1 MHz while neurons require stimulation pulses in the kHz frequency range. The analytical model for the architecture can be divided into three stages: inductive link, electrode-neuron interface and neuron (Fig. 3). In the following, analytical models for each stage of the architecture are studied and simulated in order to investigate a feasible range of practical values.

[1] Department of Bioengineering, University of California, San Diego, La Jolla, CA, USA
[2] Department of Ophthalmology, University of California, San Diego, La Jolla, CA, USA
[3] Institute for Neural Computation, University of California, San Diego, La Jolla, CA, USA

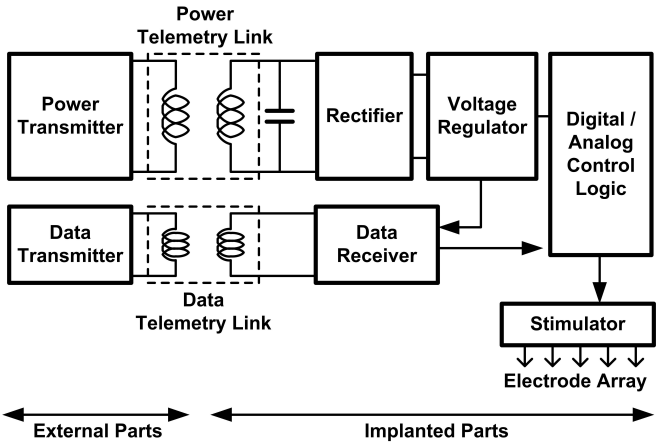

Fig. 1. Conventional architecture for wireless implanted neural stimulation.

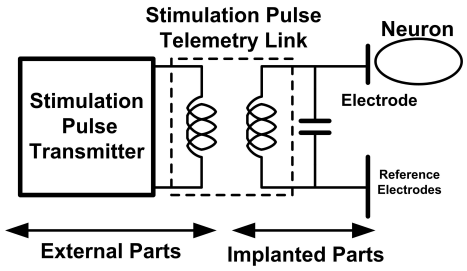

Fig. 2. Proposed architecture with direct inductive neural stimulation.

A. Analysis of Inductive Link

In most biomedical applications the primary inductor is placed externally and is less constrained than the secondary inductor, which needs to fit into the geometry of the body. The secondary coil also needs to be flexible for better contact to the tissue and needs to be insulated for biocompatiblility. Thus, microfabrication is used to achieve the required size, flexibility and biocompatibility for implantable neural stimulation.

For a prototype of the stimulator, a planar double spiral coil is patterned on a flexible substrate, and folded for two-fold increased inductance in a simple polyimide-metal-polyimide fabrication process [6]. Instead of using two metal layers [6], only one metal layer is used by placing electrodes and solder masks for electrical components in the center of the coil. The inductance L_2 and the quality factor Q_2 of the coil can be calculated with the following equations [7]:

$$L_2 = 2\frac{r^2 N^2}{20r + 28d} \quad (1)$$

978-1-4577-1787-1/12/$26.00 ©2012 IEEE

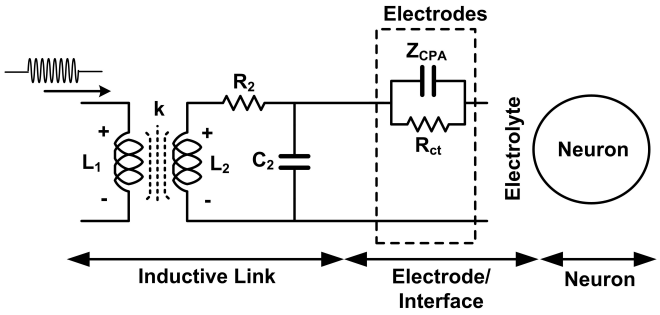

Fig. 3. Circuit model of the direct inductive stimulation.

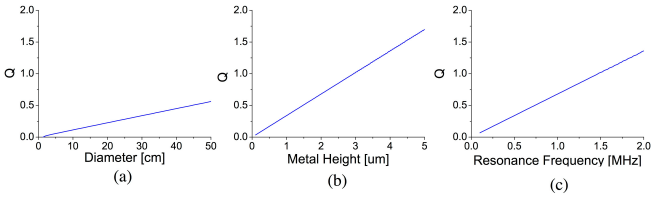

Fig. 4. Dependence of the quality factor Q on (a) coil diameter, (b) metal thickness, and (c) resonance frequency.

$$Q_2 = \frac{\omega L_2}{R_2} = \frac{\omega(2\frac{r^2N^2}{20r+28d})}{\rho\frac{2\pi rN}{wh}} \tag{2}$$

with number of windings N, mean radius of the coil r and depth d of the coil, and resistivity ρ, width w and height h of the metal line of the coil. For the practical values of each parameter (6 cm for diameter of the coil and h = 200 nm) the quality factor Q_2 is less than 0.1 at 100 kHz. For a given geometry, the number of windings does not contribute to the quality factor because $w \propto 1/N$. When either the resonance frequency is over 1.5 MHz or the height of the deposited gold layer is over 3 μm, a quality factor greater than one may be achieved. Increasing the quality factor by increasing the size of the coil is not practically achievable (Fig. 4).

B. Analysis of Electrode-Neuron Interface

A circuit model of the interface between electrode and neuron is depicted in Fig. 5. Because this study does not require subcellular spatial resolution, the point-contact model is used [8],[9] instead of the area-contact model [9]. The membrane of the neuron is divided into two domains: a free membrane and an attached junction membrane, which is close to the electrode [10],[11]. The stimulation signal is transferred to the junction membrane and the free membrane is assumed to be connected to ground. Each membrane domain is modeled here with passive elements and modeled with active elements in the next subsection. The transfer function $H(j\omega) = V_J(j\omega)/V_{STIM}(j\omega)$ for stimulation is:

$$H(j\omega) = \frac{Z_{neu}//R_{seal}}{R_{spread} + Z_{el} + Z_{neu}//R_{seal}} \frac{\frac{R_M+R_J}{1+j\omega\frac{C_{mem}}{g_{mem}}}}{Z_{neu}} \tag{3}$$

$$Z_{neu}(j\omega) = \frac{R_M + R_J}{1 + j\omega\frac{C_{mem}}{g_{mem}}} + \frac{1}{j\omega C_{hd}} \tag{4}$$

$$Z_{el}(j\omega) = Z_{CPA}//R_{ct} \tag{5}$$

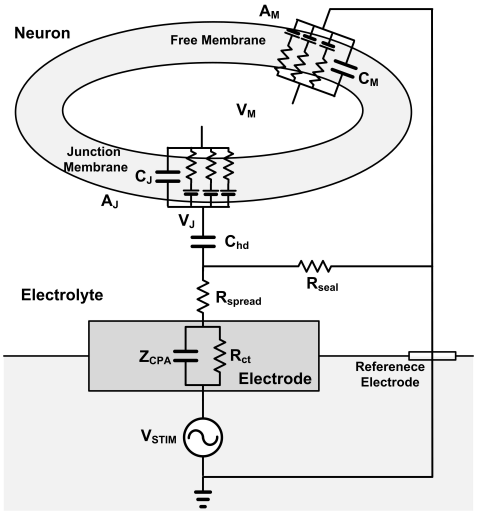

Fig. 5. Circuit model of electrode-neuron interface for neural stimulation. The parameters are defined in the appendix.

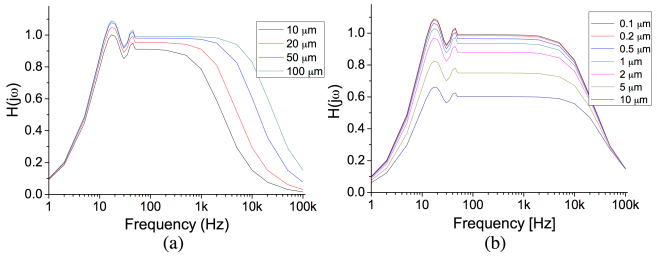

Fig. 6. Dependence of the transfer function on (a) diameter of electrode and (b) gap between electrode and neuron.

As shown in Fig. 6, the electrode-neuron interface behaves as a bandpass filter with variations in cut-off frequency and amplitude of the transfer function as a function of diameter of the electrode and the gap between the electrode and the neuron. At 100 kHz stimulation frequency, at most 20 % coupling efficiency can be achieved with practical values from the literature ([12],[13]).

C. Analysis of Neural Spike Initiation

Extracellular electrical stimulation decreases V_J, the voltage across the junction between electrode and neuron and depolarizes the membrane voltage activating sodium current flow into the cell. A train of biphasic stimuli of subthreshold amplitude has been shown to depolarize the membrane by the repetitive activation of sodium channels [11]. To study the repetitive subthreshold stimulation we consider a two-domain model with two separate membrane domains, an attached junction membrane and a free membrane. Both membranes are modeled after Hodgkin-Huxley (H-H) [14], and for the junction membrane we further consider Na^+ channels of sustained voltage-dependent conductance [15]. The limited dynamics due to the m and h variables in the H-H model does not allow effective stimulation higher than a few kHz. The faster dynamics of the sustained Na^+ conductance model suggests that 100 kHz stimulation may initiate an action

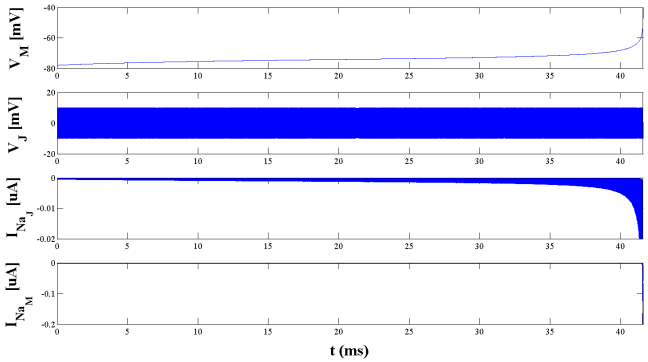

Fig. 7. Membrane and junction voltages and currents for 100 kHz stimulation pulses.

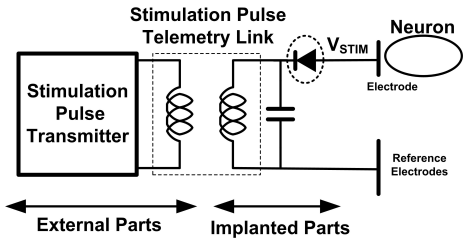

Fig. 8. Enhanced architecture with diode-rectified direct inductive neural stimulation.

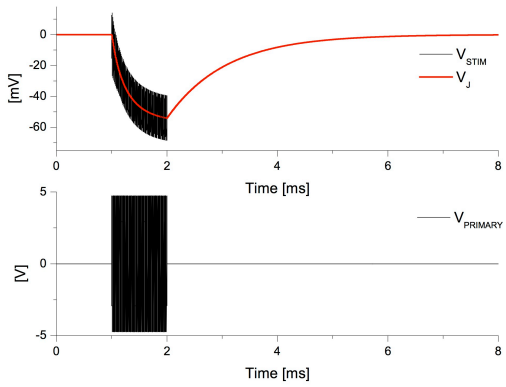

Fig. 9. Primary and neural voltage waveforms for diode-rectified direct inductive neural stimulation when the primary input signal is 10 MHz sine wave for 1 ms as shown in the bottom graph.

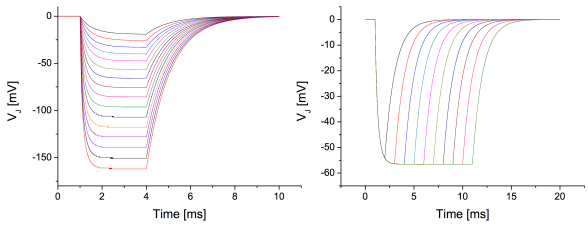

Fig. 10. The amplitude and width of the delivered stimulation pulses are controllable by changing the amplitude and number of inductive stimulation pulses.

potential by repetitive inward sodium current depolarizing membrane voltage as shown in Fig. 7. However, even if 100 kHz neural stimulation can be effective, it is still out of the practical range for high-Q inductive stimulation.

III. Rectified Direct Inductive Stimulation

The previous section establishes that direct inductive neural stimulation is not practically feasible. However, accounting for rectification and lowpass filtering in between the secondary coil and the membrane junction, it is possible to bridge the gap between the optimal frequency ranges for high-Q induction and neural stimulation. We model rectification as an explicit diode shown in Fig. 8, however the rectification may be intrinsic to the electrode and the membrane junction. For instance, our previous work shows such rectification in a PN-junction nanowire array for photoconductive and neural stimulation in a retinal prosthesis [16].

The modeled diode serves to rectify the incoming sine wave to generate a monophasic voltage pulse, which causes balanced charge injection in the limit of capacitive rather than ohmic coupling to the tissue [11]. Fig. 9 illustrates neural stimulation with a 1 ms, 10 MHz sine pulse from the external transmitter. The strength and width of the pulse on the junction are individually controlled by changing the amplitude and number of pulses of the primary input voltage in the external part (Fig. 10).

IV. Proof of Concept Prototype

The coils were patterned on and encapsulated within polyimide as noted in Section II-A. The planar structure of one flexible coil prior to folding is illustrated in Fig. 11. Building this prototype required investigating the optimal coil design, inductive pulse duration and frequency to produce reliable neural stimulation waveforms. Although the design cannot produce conventional square wave neural stimulation waveforms, recent work indicates square waveform may not be the most ideal waveform for reproducible neural activation. In the following we outline our device fabrication and initial proof of concept experiments.

Flexible coil fabrication: Polyimide was spun on silicon wafer with a thickness of 10 μm (Pyralin PI 2611, HD Microsystems). Polyimide was cured according to specifications, briefly temperature ramp at 5 ^{o}C/minute until 375 ^{o}C where the wafer was left at that temperature for an hour. Ebeam evaporator was used to deposit 200 nm of gold with 10nm chrome adhesion layer. Photoresist was spun and exposed using a chrome mask, and developed to produce the desired after etching with gold and chrome etch. Insulation for the coils was done using photopatentable polyimide which was spun on the pattern for a thickness of 5 μm.

Retina tissue prep: The retina was the choice tissue for proof of concept experiment in support of our retinal prostheses work [16]. An adult rat was euthanized with carbon dioxide. Eyes were excised with a straight forceps and placed in Ringer solution bubbled with 95% O_2 / 5% CO_2 at a temperature of 30 ^{o}C. The Ringers solution contains (in mmol/L): 117.0 NaCl, 3.0. KCl, 2.0 $CaCl_2$, 1.0 $MgSO_4$,

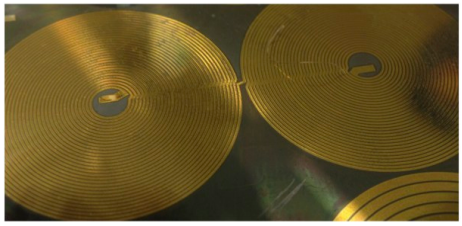

Fig. 11. Flexible substrate microfabrication of secondary coils for direct inductive neural stimulation.

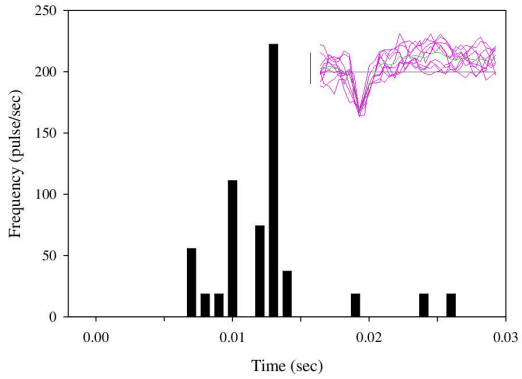

Fig. 12. PSTH for 6 neurons firing in response to rectified stimuli at 5 ms duration and 160 mV pulse amplitude. Inset: overlaid recorded spike waveforms with scale bars at 60 μV and 1.6 ms.

0.5 NaH_2PO_4, 15.0 D-glucose, 32 $NaHCO_3$, and 0.01 L-glutamate. The eye cup was perforated and cut around the ora serrata with a surgical scissor. The lens was removed and the retina loosened from the sclera with fine forceps, with care not to touch the retina to minimize damage. The dissection was performed under dissection microscope (retina is bleached). The retina was then moved to a Microelectrode array (64 channel MEA, Multichannel System, Germany) by mounting on filter paper and then placed ganglion side down. The retina was left for 15 minutes in continuously perfused oxygenated Ringers solution. The retina was bleached prior to experiment with a surgical light for 5 minutes.

V. Results

The rectified generated pulses in Fig. 10 were loaded through Labview and the analog output was used to stimulate the retina via one of the MEA channels. The results in Fig. 12 show peristimulus time histogram (PSTH) for 6 ganglion cells responding to 6 stimulation pulses showing proof of concept. Work in progress will further characterize total charge injected by the proposed waveforms and how it compares to basic square pulses typically used in neural stimulation.

VI. Conclusion

This work investigates a simplified neural stimulation architecture that relies on direct inductive link to produce a tunable neural stimulation waveform. Our modeling and experimental data show the feasibility of the concept and potential for use in neural stimulation. The concept can be directly extended to multi-site neural stimulation with a single inductive link through localized optical control, such as by light-induced conductance in an array of nanowire electrodes for high-resolution retinal prostheses [16]. Future work will aim at optimizing the stimulation waveform (coils dimensions, inductive link waveform) for reliable neural stimulation that will be dictated by the target neural tissue.

APPENDIX

A_M: area of the free membrane, A_J: area of the junction membrane, C_M: capacitance of the free membrane, C_J: capacitance of the junction membrane, R_M: membrane resistance of the free membrane, R_J: membrane resistance of the junction membrane, V_M: intracellular voltage, V_J: junction voltage, C_{hd}: membrane-electrolyte interface capacitance, R_{seal}: sealing resistance, R_{spread}: spreading resistance, Z_{CPA}: constant phase angle impedance, R_{ct}: faradic charge transfer resistance, C_{mem}: membrane capacitance per unit area, g_{mem}: membrane conductivity per unit area.

References

[1] B. K. Thurgood *et al.*, "A wireless integrated circuit for 100-channel charge-balanced neural stimulation," *IEEE Transactions on Biomedical Circuits and Systems*, vol. 3, no. 6, 2009.

[2] K. Chen *et al.*, "An integrated 256-channel epiretinal prosthesis," *IEEE Journal of Solid-State Circuits*, vol. 45, no. 9, 2010.

[3] S. K. Arfin and R. Sarpeshkar, "An Energy-Efficient, Adiabatic Electrode Stimulator With Inductive Energy Recycling and Feedback Current Regulation," *IEEE Transactions on Biomedical Circuits and Systems*, vol. 6, no. 1, 2012.

[4] B. Ziaie *et al.*, "A single-channel implantable microstimulator for functional neuromuscular stimulation," *IEEE Transactions on Biomedical Engineering*, vol. 44, no. 10, 1997.

[5] H.-W. Chiu *et al.*, "Pain control on demand based on pulsed radio-frequency stimulation of the dorsal root ganglion using a batteryless implantable CMOS SoC," *IEEE Transactions on Biomedical Circuits and Systems*, vol. 4, no. 6, 2010.

[6] W. Lia *et al.*, "Parylene-based integrated wireless single-channel neurostimulator," *Sensors and Actuators A: Physical*, vol. 166, no. 2, 2011.

[7] H. A. Wheeler, "Simple inductance formulas for radio coils," *Proceedings of the Institute of Radio Engineers*, vol. 16, no. 10, 1928.

[8] P. Fromherz, "Neuroelectronic Interfacing: Semiconductor Chips with Ion Channels, Nerve Cells and Brain," *Nanoelectronics and Information Technology*, 2003.

[9] N. Joye *et al.*, "An electrical model of the cell-electrode interface for high-density microelectrode arrays," *Proceedings of 30th Annual International Conference of the IEEE EMBS*, 2008.

[10] R. Weis and P. Fromherz, "Frequency dependent signal transfer in neuron transistors," *Physical Review E*, vol. 55, no. 1, 1997.

[11] I. Schoen and P. Fromherz, "Extracellular stimulation of mammalian neurons through repetitive activation of Na^+ channels by weak capacitive currents on a silicon chip," *Journal of Neurophysiology*, vol. 100, 2008.

[12] W. Franks *et al.*, "Impedance characterization and modeling of electrodes for biomedical applications," *IEEE Transactions of Biomedical Engineering*, vol. 52, no. 7, 2003.

[13] J. R. Buitenweg *et al.*, "Geometry-based finite-element modeling of the electrical contact between a cultured neuron and a microelectrode," *IEEE Transactions of Biomedical Engineering*, vol. 50, no. 4, 2003.

[14] A. L. Hodgkin and A. F. Huxley, "A quantitative description of membrane current and its application to conduction and excitation in nerve," *Journal of Physiology*, vol. 117, 1952.

[15] M. F. Sheets and D. A. Hanck, "Gating of skeletal and cardiac muscle sodium channels in mammalian cells," *Journal of Physiology*, vol. 514, pt. 2, 1999.

[16] M. L. Khraiche *et al.*, "Ultra-high photosensitivity silicon nanophotonics for retinal prosthesis: electrical characteristics," *Proceedings of the 33rd Annual International Conference of the IEEE EMBS*, 2011.